

# *In vivo* cellular optical coherence tomography imaging

STEPHEN A. BOPPART<sup>1,2</sup>, BRETT E. BOUMA<sup>1</sup>, COSTAS PITRIS<sup>1,2</sup>, JAMES F. SOUTHERN<sup>3</sup>,  
MARK E. BREZINSKI<sup>4</sup> & JAMES G. FUJIMOTO<sup>1</sup>

<sup>1</sup>Department of Electrical Engineering and Computer Science, Research Laboratory of Electronics, Massachusetts Institute of Technology, 77 Massachusetts Avenue, Room 36-345, Cambridge, Massachusetts 02139, USA

<sup>2</sup>Harvard-MIT Division of Health Sciences and Technology; MIT, Cambridge, Massachusetts 02139, USA

<sup>3</sup>Pathology Department, The Children's Hospital, Boston, Massachusetts 02115, USA

<sup>4</sup>Cardiac Unit, Harvard Medical School, Massachusetts General Hospital, Boston, Massachusetts 02114, USA

Correspondence should be addressed to J.G.F.

Neoplasias are most responsive to medical intervention at early stages, prior to undergoing metastasis. When these disorders arise from known premalignant states, and if a detection method exists, the high-risk population can be screened to reduce patient morbidity and mortality. Organs where these premalignant conditions occur at relatively high frequency include the esophagus, uterus, bladder, colon and stomach. The ability to image pathology in these organs at cellular resolutions, *in situ* and in real time, without the need to excise and process specimens, could represent a powerful tool for the early identification of neoplasms. New technologies that have been pursued, with limited success, for the high-resolution assessment of cellular structure include magnetic resonance imaging (MRI)<sup>1</sup>, X-ray microscopy<sup>2</sup> and high-frequency ultrasound<sup>3</sup>. Although cellular imaging has been generated with MRI of small organisms, these resolutions have not been reproduced in humans. Furthermore, the image acquisition rates are prohibitively long for most clinical applications. X-ray microscopy has superior resolution to conventional microscopy due to the shorter wavelengths of the incident electromagnetic radiation. However, long data acquisition rates and hazards associated with high-energy radiation makes this technique impractical for routine clinical use. High-frequency ultrasound transducers (30 MHz) are now in clinical use which have a resolution of approximately 110  $\mu\text{m}$ . However, clinical imaging at resolutions necessary for cellular-level discrimination has not been achieved with this relatively mature technology. Furthermore, ultrasound imaging requires either direct contact with the tissue or a transducing medium, which is impractical for screening large areas of tissue. Confocal microscopy has been an important advance in microscopy and enables the imaging of intact, optically non-transparent specimens. Recently, investigators have demonstrated high-speed, *in vivo*, laser-scanning confocal microscopy for imaging cellular morphology in skin<sup>4</sup>. Confocal microscopy produces high-resolution images of tissue cross-sectional structure, but imaging depths are limited to a few hundred microns.

Optical coherence tomography (OCT)<sup>5</sup>, a new method of micron-scale endoscopic based imaging, has the potential for overcoming the limitations of these technologies. OCT is analogous to ultrasound, measuring the intensity of backreflected infrared light rather than sound waves. It is a technique that combines the high resolutions of most optical techniques with an ability to reject multiply scattered photons and, hence, image at cellular resolutions up to millimeters deep in non-transparent tissue. Image penetration is enhanced by using high-sensitivity, interferometric-based detection techniques and performing imaging at near-infrared wavelengths, which are absorbed and scattered less than shorter, visible wave-

lengths. Because OCT relies on variations in index of refraction and optical scattering for image contrast, no exogenous fluorophores are necessary for imaging. Thus, imaging cells within living specimens is possible without loss of viability. Imaging can be performed over extended periods of time in single specimens to assess cell size or mitotic activity. OCT technology was originally applied to imaging the transparent structures of the eye and is promising for the diagnosis of retinal diseases<sup>6,7</sup>. It has also been shown to be effective at imaging in more highly scattering tissue such as the skin and cardiovascular system<sup>8-10</sup>. Recently, studies have demonstrated imaging of *in vivo* rabbit respiratory and gastrointestinal tracts using a high-speed, endoscope-based OCT system<sup>11</sup>.

Although previous studies have demonstrated *in vivo* OCT imaging of tissue morphology, most have imaged tissue at ~10–15  $\mu\text{m}$  resolutions, which does not allow differentiation of cellular structure. In this manuscript, the *Xenopus laevis* (African frog) tadpole, a common developmental biology animal model, is used to demonstrate the feasibility of OCT for *in vivo* cellular imaging. The ability of OCT to identify the mitotic activity, the nuclear-to-cytoplasmic ratio, and the migration of cells is evaluated. OCT images are compared to corresponding histology to verify identified structures. Optical coherence tomography provides images of tissue morphology on a level approaching that of conventional histology, but permits imaging to be performed *in vivo* and *in situ* without the need to excise and process specimens. *In situ* and *in vivo* imaging of cellular morphology has the potential for a wide range of applications ranging from developmental biology research to clinical applications such as the screening and diagnosis of neoplastic changes.

## *In vivo* cellular implications

A comparison between OCT images and corresponding histology is shown in Fig. 1. The comparison between Fig. 1a and b confirms the presence of multiple nuclei and cell membranes. The seemingly wide cell membranes in the OCT images are actually composed of membranes and extracellular matrix. Some variation in the correspondence between OCT and histology exists in Fig. 1a and b, most likely due to small angular deviations in the histological sectioning plane. The OCT image in Fig. 1a illustrates cells with varying size and nuclear-to-cytoplasmic ratios. Based on image measurements, cells as small as 10  $\mu\text{m}$  in diameter can be imaged. An enlarged OCT image of a dividing cell is shown in Fig. 1c with corresponding histology in Fig. 1d. Two distinct nuclei are clearly shown. To the right of the nuclei, the membrane has begun to pinch in. The OCT image in Fig. 1e demonstrates the high backscattering observed from melanin contained within neural crest melanocytes and tissue structures. Two melanocytes located within the superficial membrane are

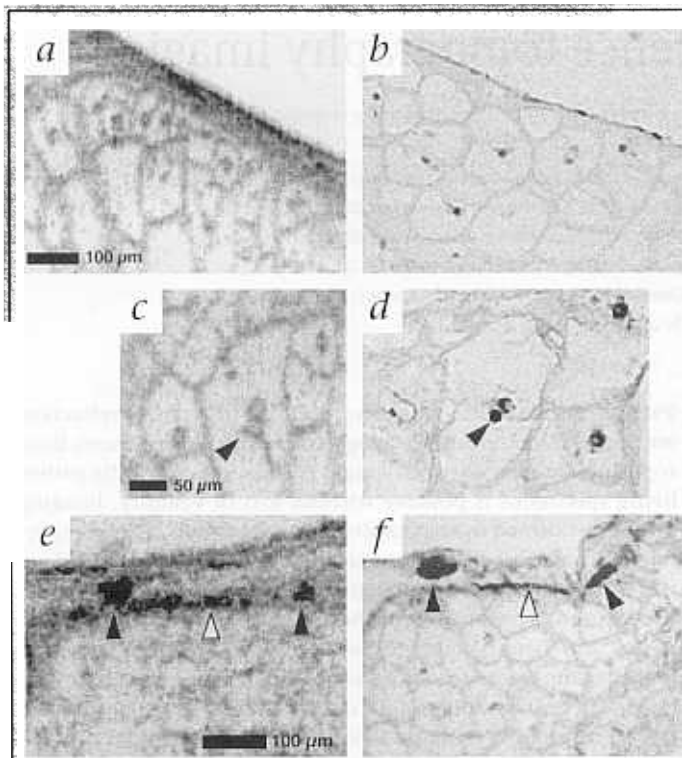


**Fig. 1** Comparison to histology. Histological preparations stained with hematoxylin and eosin correlate cellular structures with OCT images. **a** and **b**, Mesenchymal cells of various size and nuclear-to-cytoplasmic ratios. Exact cellular matches were difficult to achieve at these dimensions. **c** and **d**, Enlarged image of dividing cell correlates well with histology. Pinching membrane and nuclei are observed. **e** and **f**, OCT image and corresponding histology of neural crest cells (black arrows) containing melanin. Melanin appears highly backscattering in OCT images and can be detected through scattering, non-transparent issue. Additional melanin pigment layer is observed (white arrow).

separating them. The remaining figures (Fig. 2d-f) show the increasing separation of the nuclei and the growth in cell size.

Although not directly relevant to clinical imaging, the capability of monitoring cell migration through an organism would be a powerful tool in a variety of developmental and molecular models. The ability of OCT to track individual cell movement is illustrated in Fig. 3. A neural crest melanocyte (m) in Fig. 3a, was imaged at 10-min intervals by acquiring three-dimensional (3-D) volumes containing the cell. From each volume, the 2-D cross-section acquired through the center of the cell is shown in Fig. 3. Because of slight changes in specimen movement over time, internal morphological features and markers within the image were used as reference points. The top arrow in Fig. 3a indicates the outer membrane of the specimen whereas the left arrow indicates a melanin layer covering the dorsal neural tube. Each was used as an internal reference point.

A 3-D plot of cell position within the specimen is shown in Fig. 4. The *x* and *y* Cartesian coordinates were determined from the image measurements obtained in Fig. 3a-f. The *z* coordinate was determined from the cell movement between planes of the 3-D volume. The points labeled a-f correspond to the images shown in Fig. 3. The cell migration between each labeled point corresponds to 10-min intervals. This plot indicates the cell migrated along a curved path progressing first dorsolaterally and then dorsomedially. Projections of the migration are also shown in Fig. 4 in the transverse, coronal, and sagittal planes.

indicated by black arrows while a melanin layer from the pigmentation pattern is indicated by the white arrow. The corresponding histology in Fig. 1f verifies these observations.

In order to confirm the ability of OCT to identify cell division further, a sequence of OCT images following the mitotic activity of a single cell is shown in Fig. 2. A large number of mesenchymal cells are observed within each image. These undifferentiated cells range in size from 100 μm down to sizes below the resolution of OCT. Cell nuclei and cell membranes are readily apparent as regions of high backscatter compared with the low backscattering cytoplasm. A number of cells show sub-nuclear morphology, such as the regions of increased optical backscatter within the nucleus in Fig. 2a. One possibility is that these are regions of varying chromatin concentration, indicative of high mitotic activity. Future studies are necessary to clarify this observation further.

Within each image, cells can be found in various stages of mitosis and exhibit a high degree of pleomorphism. Mitotic activity of one parent mesenchymal cell and the migration of the two daughter cells is shown in the sequence of Fig. 2a-f. The parent cell (arrow) in Fig. 2a is in telophase and the chromosomes appear to have reached the mitotic poles. The membrane in the upper left of this cell has begun to pinch in. Ten minutes later, in Fig. 2b, there is more distinct separation and the appearance of two adjacent nuclei. After an additional 10 min, the two daughter cells in Fig. 2c have a distinct membrane

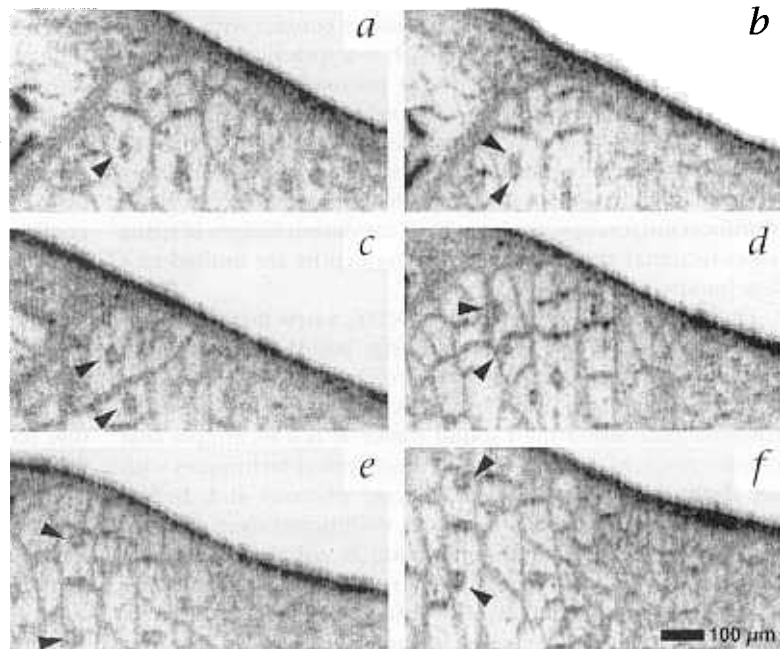


**Fig. 2** Sequence of mitotic division. OCT images collected from a single *in vivo* specimen demonstrate mitotic activity in differentiating mesenchymal cells. **a**, Parent cell (arrow) with signs of membrane pinching and chromatin clumping. **b**, Early separation (two arrows) with possible spindles. **c-f**, Two distinct migrating and growing daughter cells (two arrows). Images were acquired at 10-min intervals.

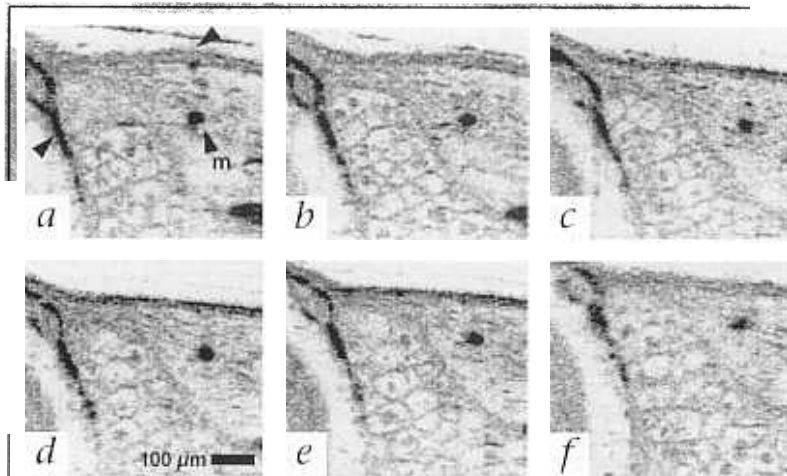


**Fig. 3** Cell migration. Sequence demonstrates tracking of a neural crest melanocyte (m) through tissue. Position was determined using Cartesian coordinates relative to the outer membrane and melanin layer (black arrows). Images were acquired at 10-min intervals.

### Clinical research implications

In this paper, high-resolution, cellular level OCT imaging was demonstrated in a non-transparent animal model. OCT yields cross-sectional images with a resolution approaching that of conventional histopathology, but without the need for excision and processing of tissue specimens. Thus, imaging can be performed *in situ*, *in vivo*, and in real time. In addition, because imaging is performed without the need for excision of a specimen, large areas of tissue can be imaged, thereby overcoming the sampling limitations of conventional excisional biopsy. These results suggest the feasibility for a wide range of potential applications ranging from developmental biology to clinical applications, such as assessing neoplastic changes in humans. The observations of greatest clinical relevance were the ability to identify active cell division and to assess empirically relative nuclear-to-cytoplasmic ratios, two important markers of malignant transformation. Both observations were correlated with histopathology. In addition, to confirm the ability of identifying cell division further, a single cell was followed through a single division cycle and changes in morphology were noted. A change in the backscattering intensity from nuclei was also noted as a function of time. This is postu-

lated to represent a change in the concentration or packing of chromatin, which may be of diagnostic relevance. However, this observation requires more rigorous evaluation to confirm its origin.

The *Xenopus* developmental animal model was selected because it is a well established, extensively studied model and displays a wide range of cell sizes, which also have a high degree of mitotic activity. Many of the cells observed were as large as 100  $\mu\text{m}$  in diameter, but ranged in size down to dimensions below the resolution of this OCT system. This provided an evaluation of the cell size limits that could be imaged using OCT and a basis for extrapolating imaging performance. At current OCT imaging resolutions, cells as small as 10  $\mu\text{m}$  in diameter could be imaged. The size of most malignant cells in humans varies dramatically, showing an approximate correlation with the degree of differentiation. Normal, differentiated human cells may be as small as 5  $\mu\text{m}$ , but cell dimensions found in human neoplasias are typically in the range of 10–40  $\mu\text{m}$  and therefore similar in size to the cells imaged in this animal model. Cell sizes are larger in high-grade dysplasias and neoplasias, however in low-grade dysplasias, cell size tends to be smaller and will be more difficult to resolve using OCT imaging at the current 5- $\mu\text{m}$  resolution level. Future studies will focus on *in vitro* and *in vivo* imaging of human cells in normal, dysplastic, and neoplastic tissues.

Technical milestones anticipated in OCT development include improvements in endoscope design and increasing data acquisition rates. OCT imaging is achieved over a distance of 2 to 3 mm, which is roughly the size of a conventional excisional biopsy. It can be performed at almost any site in the body through small fiber-optic endoscopes. *In vivo* OCT imaging of the rabbit circulatory, gastrointestinal, and respiratory systems has been performed through a 1-mm diameter OCT imaging endoscope<sup>11</sup>. It is anticipated that future modifications will allow the diameter of the endoscope to be reduced substantially. The data acquisition rate in this study was not optimal for *in vivo* imaging. *In vivo* studies have been performed with imaging at 4–8 frames/second at lower resolutions<sup>12</sup>. However, at 5- $\mu\text{m}$  resolution, this acquisition rate is currently not available. Future studies will focus on increasing data acquisition rates at high resolutions. Near-video acquisition rates should ultimately be possible.

Data in this paper were interpreted via an empiric correlation with histology. Interpretation of data was also facilitated by the fact that comprehensive OCT image data were taken corresponding to multiple cross-sectional planes covering 3-D volumes of tissue as a function of time. This permitted the imaging of cell activity throughout the entire mitotic cycle, as well as the tracking of dynamic changes such as cell shape and migration. The free space axial resolution in this study was 5.1  $\mu\text{m}$  and is governed by the spectral bandwidth of the laser source. The actual resolution in tissue varies as a function of the depth being imaged, as well as the optical properties of the tissue. No attempts were made to quantify resolution within tissue. Near the surface, the predicted axial resolution is actually higher than 5.1  $\mu\text{m}$ . The

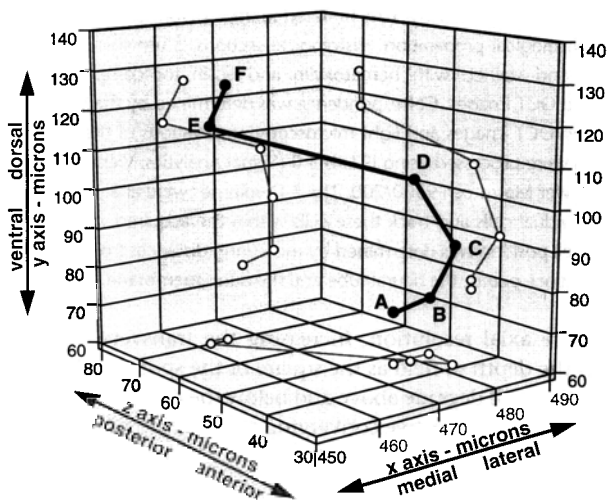


**Fig. 4** Three-dimensional tracking of neural crest melanocyte migration. Three-dimensional volumes were acquired at 10-min intervals. Cell locations were determined from image measurements described in Fig. 3 and from position in 3-D volume. The letter sequence (A–F) corresponds to position of the cell over time. Projections of the migration are also shown in the transverse, coronal, and sagittal planes.

## Methods

**Optical coherence tomography.** The principles and physics of OCT have been previously described in detail<sup>1</sup>. OCT is somewhat analogous to ultrasound B-mode imaging, except backscattering of light is detected rather than sound. Whereas ultrasound pulse propagation and detection can be described in terms of time delays, the echo delay time of light returning to the OCT instrument from the specimen cannot be measured directly by electronic methods due to the high speeds associated with the propagation of light. Therefore, a technique known as interferometry is used, which utilizes a reference and a sample arm. A schematic of the fiber-optic based Michelson interferometer, which allows measurements of precise depth and magnitude of each reflection, is shown in the schematic diagram.

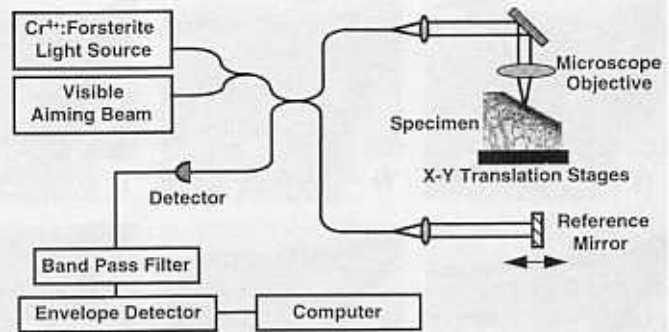
With Michelson interferometry, light is split equally by a fiber coupler with half sent to the reference arm and half sent to the sample arm of the interferometer. A mechanical, scanning reference arm mirror sets the depths at which backscatter will be measured and induces a known Doppler-shift in the returned light. Reflections or backscatter from the specimen are combined with reflected light from the reference arm by the fiber coupler, detected by a photodiode, and electronically filtered around the Doppler-shifted frequency. Interference between the two arms occurs only when their path lengths are matched to within the coherence length of the source.

The axial resolution is determined by the coherence length of the source. A free-space axial resolution of 5.1  $\mu\text{m}$  was determined by measuring the point-spread function from a mirror placed in the sample arm. The transverse resolution is determined by the spot size of the incident beam within the tissue. The spot size in free-space was 9  $\mu\text{m}$ , which yielded a 100  $\mu\text{m}$  confocal parameter (depth of field). The confocal parameter for the beam was selected to match axial and transverse resolutions closely while maintaining a sufficient depth of field.

The signal-to-noise ratio was 110 dB using 2 mW of incident power on the specimen. For typical tissues, this sensitivity permits imaging to depths of 2–3 mm. Images were generated by assembling adjacent axial scans to form a 2-D cross-sectional image of the specimen. Data were displayed as the logarithm of the backscattered intensity versus position in gray-scale. Acquisition time for a single axial scan was 33 ms. The incident beam was scanned in the transverse direction to acquire the OCT image. Imaging was performed using 300 axial scans and the acquisition time per image was therefore 10 s. A Kerr-lens mode-locked, solid-state Cr<sup>4+</sup>:forsterite laser operating at 1280 nm center wavelength was used as a broad bandwidth source<sup>15</sup>.

**Specimen preparation and imaging.** *Xenopus laevis* embryos were acquired 1 h after fertilization and maintained in a solution of 1/10  $\times$  MBS (Modified Barth's Saline) at room temperature with a 12 h light–dark cycle. Tadpoles were fed a prepared diet of *Xenopus* Nutrient (Connecticut Valley Biological, Southamptton, Massachusetts) once daily. The animals used in this study were cared for and maintained under the established protocols of

predicted *in vivo* axial resolution is the free-space resolution of the system divided by the index of refraction. An average index of refraction ( $n = 1.35$ ) was determined for these *Xenopus* specimens by measuring the optical thickness of the specimen using OCT and comparing it to the actual thickness<sup>13</sup>. The measured index is very close to that of water ( $n = 1.33$ ), the main constituent of the specimen, but represents an average value because the specimens are inhomogeneous. The predicted *in vivo* axial resolution is therefore 5.1  $\mu\text{m}/1.35 \sim 3.8 \mu\text{m}$ . At increasing depths within the tissue, the axial resolution deteriorates because light is multiply scattered<sup>14</sup>. The transverse resolution is determined by the focusing characteristics of the beam-delivery optics and is independent



Schematic of the OCT instrument. Light from a Cr<sup>4+</sup>: forsterite laser is split equally and sent down sample and reference arms of the fiber-optic interferometer. Reflections from the mirror and specimen are recombined and detected. By translating the specimen, 3-D volumes of image data representing optical backscatter intensity can be collected.

the MIT Committee on Animal Care.

Five specimens were imaged for this *in vivo* study. Specimens ranged in age from 14–28 days (stage 25–30)<sup>16</sup>. Specimens were anesthetized by immersion in 0.05% Tricaine for 5 min until they no longer responded to touch. Imaging was performed by orienting the specimen so the light beam from the OCT sample arm was incident on the dorsal side as the specimen rested in a clay-lined Petri dish. The specimen was aligned beneath the microscope objective using a three-axis, computer-controlled, micron-precision stage. The position of the invisible infrared OCT beam (1280 nm) on the specimen was monitored with a coincident visible guiding beam (632 nm). Drops of housing-tank medium were placed over the specimen at 5-min intervals to prevent dehydration during imaging. Multiple 2-D cross-sections (900  $\times$  600  $\mu\text{m}$ , 300  $\times$  300 pixels) were acquired perpendicular to the anteroposterior axis. Fifteen 2-D cross-sections acquired at 5- $\mu\text{m}$  intervals were assembled to produce a 3-D dataset. Three-dimensional volumes were acquired every 10 min from the region posterior to the eyes and lateral to the neural tube of the specimen.

Immediately following image acquisition, the location of the image planes was marked with India ink for registration between OCT images and histology. Specimens were euthanized by immersion in 0.05% Benzocaine for 1 h and then placed in a 10% buffered solution of formaldehyde for standard histological preparation. Histological sections, 5- $\mu\text{m}$  thick, were sectioned and stained with hematoxylin and eosin for comparison with acquired OCT images. Correspondence was determined by the best match between OCT images and light microscopy observations of the histology. Images were processed using IP Lab 3.0 (Signal Analytics, Vienna, Virginia) on a Power Macintosh 9500/200. The 3-D volumes were analyzed to identify individual cells and track these cells within the acquired volumes over time. Cell position was determined by measuring distances from two internal reference points, the neural tube and the outer membrane.

from the axial resolution. Increasing the transverse resolution limits the depth of field as the square of the spot size. Transverse resolution will degrade above and below the depth of field region because of the respective converging and diverging optical beam. This phenomenon is analogous to the depth of field limitations encountered in conventional optical microscopy. In addition, reductions in transverse resolution are anticipated to occur due to wavefront aberrations and forward scattering. However, based on the empiric assessment of the images generated, cellular resolution appears to exist throughout these image depths.

The resolution of OCT imaging will be an important factor in determining its ultimate range of clinical applications, includ-

ing its potential for detection of neoplasias. Further improvements in resolution are possible. Axial image resolution is directly determined by the wavelength bandwidth of the light source, and with the development of broader bandwidth sources, increases in resolution down to the 2- $\mu\text{m}$  scale should be feasible. The transverse resolution may also be improved by changing the focusing parameters of the optical beam, but increasing transverse resolution will trade off against decreasing depth of focus. Tissue optical properties, especially optical scattering and aberration effects, will also play a role in determining the ultimate limitations to OCT image resolution and further investigation of these effects is needed.

In conclusion, the results reported demonstrate high-resolution, cellular level OCT imaging, including the assessment of mitotic activity and relative nuclear-to-cytoplasm ratios. OCT imaging can be performed *in situ*, *in vivo*, and in real time without the need for excision and processing of tissue specimens. Because imaging is performed without the need for excision of a specimen, large areas of tissue can be imaged, thereby overcoming the sampling limitations of conventional excisional biopsy. These results suggest the feasibility for clinical applications such as assessing neoplastic changes in humans. In addition, the ability to track cell movement may offer insight into fundamental developmental biology research, as well as offer the ability to assess *in vivo* tumor invasion and growth.

#### Acknowledgments

The authors would like to thank Hazel Sive and her laboratory personnel at MIT for providing us with specimens and advice on the care and handling of embryos. We would also like to acknowledge the technical input from Eric A. Swanson of MIT Lincoln Laboratory and Gary Tearney of the Harvard Medical School. Brett Bouma is currently with the Wellman Laboratory of the Massachusetts General Hospital. This research is supported in part by grants from the Office of Naval Research, Medical Free Electron Laser Program,

Grant N00014-97-1-1066, the National Institutes of Health, Contracts NIH-1-RO1-CA75289-01 (J.G.F. & M.E.B.), NIH-1-R29-HLS5686-01A1 (M.E.B.), NIH-RO1-AR44812-01 (M.E.B.), the Whittaker Foundation Contract 96-0205 (M.E.B.), the Air Force Office of Scientific Research, Grant F49620-95-1-0221, and the Air Force Palace Knight Program.

1. Jacobs, R.E. & Fraser, S.E. Magnetic resonance microscopy of embryonic cell lineages and movements. *Science* **263**, 681–684 (1994).
2. Rajyaguru, J.M., Kado, M., Nekula, K., Richardson, M.C. & Muszynski, M.J. High-resolution X-ray micrography of live *Candida albicans* using laser plasma pulsed point X-ray sources. *Microbiology* **143**, 733–738 (1997).
3. Turnbull, D.H., Bloomfield, T.S., Baldwin, H.S., Foster, F.S. & Joyner, A.L. Ultrasound backscatter microscope analysis of early mouse embryonic brain development. *Proc. Natl. Acad. Sci. USA* **92**, 2239–2243 (1995).
4. Rajadhyaksha, M., Grossman, M., Esterowitz, D., Webb, R.H. & Anderson, R.R. *In vivo* confocal scanning laser microscopy of human skin: Melanin provides strong contrast. *J. Invest. Dermatol.* **104**, 946–952 (1995).
5. Huang, D. *et al.* Optical coherence tomography. *Science* **254**, 1178–1181 (1991).
6. Hee, M.R. *et al.* Optical coherence tomography of the human retina. *Arch. Ophthalmol.* **113**, 326–332 (1995).
7. Puliafito, C.A. *et al.* Imaging of macular diseases with optical coherence tomography. *Ophthalmology* **120**, 217–229 (1995).
8. Schmitt, J.M., Yadlowsky, M. & Bonner, R.F. Subsurface imaging of living skin with optical coherence microscopy. *Dermatology* **191**, 93–98 (1995).
9. Brezinski, M.E. *et al.* Optical coherence tomography for optical biopsy: Properties and demonstration of vascular pathology. *Circulation* **93**, 1206–1213 (1996).
10. Fujimoto, J.G. *et al.* Optical biopsy and imaging using optical coherence tomography. *Nature Med.* **1**, 970–972 (1995).
11. Tearney, G.J. *et al.* *In vivo* endoscopic optical biopsy with optical coherence tomography. *Science* **276**, 2037–2039 (1997).
12. Boppart, S.A. *et al.* Noninvasive assessment of the developing *Xenopus* cardiovascular system using optical coherence tomography. *Proc. Natl. Acad. Sci. USA* **94**, 4256–4261 (1997).
13. Boppart, S.A., Brezinski, M.E., Bouma, B.E., Tearney, G.J. & Fujimoto, J.G. Investigation of developing embryonic morphology using optical coherence tomography. *Dev. Biol.* **177**, 54–64 (1996).
14. Schmitt, J.M., Knuttel, A., Yadlowsky, M. & Eckhaus, M.A. Optical coherence tomography of a dense tissue: Statistics of attenuation and backscattering. *Phys. Med. Biol.* **39**, 1705–1720 (1994).
15. Bouma, B.E., Tearney, G.J., Bilinsky, I.P., Golubovic, B. & Fujimoto, J.G. Self-phase modulated Kerr-lens modelocked Cr:forsterite laser source for optical coherence tomography. *Opt. Lett.* **21**, 1839–1841 (1996).
16. Nieuwkoop, P.D. & Faber, J. in *Normal Table of Xenopus laevis*. (Garland Publishing, New York, NY).